Acta Crystallographica Section D
Biological Crystallography
ISSN 0907-4449

Quantifying X-ray radiation damage in protein crystals at cryogenic temperatures

Jan Kmetko,*‡ Naji S. Husseini, Matthew Naides, Yevgeniy Kalinin and Robert E. Thorne

Physics Department, Cornell University, Ithaca, NY 14853, USA

‡ Present address: Physics Department, Kenyon College, Gambier, OH 43022, USA.

Correspondence e-mail: kmetkoj@kenyon.edu

Received 4 January 2006
Accepted 23 June 2006

The dependence of radiation damage to protein crystals at cryogenic temperatures upon the X-ray absorption cross-section of the crystal has been examined. Lysozyme crystals containing varying heavy-atom concentrations were irradiated and diffraction patterns were recorded as a function of the total number of incident photons. An experimental protocol and a coefficient of sensitivity to absorbed dose, proportional to the change in relative isotropic B factor, are defined that together yield a sensitive and robust measure of damage. Radiation damage per incident photon increases linearly with the absorption coefficient of the crystal, but damage per absorbed photon is the same for all heavy-atom concentrations. Similar damage per absorbed photon is observed for crystals of three proteins with different molecular sizes and solvent contents.

1. Introduction

X-ray radiation damage to biological crystals during data collection can be a major obstacle in macromolecular structure determination (Blake & Phillips, 1962; Helliwell, 1988; Gonzalez & Nave, 1995; Nave, 1995; Glaeser *et al.*, 2000; Garman & Nave, 2002; Nave & Garman, 2005). The amount of radiation damage incurred in collecting a data set depends upon the parameters of the experimental setup such as X-ray beam size and shape (Schulze-Briese *et al.*, 2005), wavelength (Arndt, 1984; Helliwell, 1988; Polikarpov *et al.*, 1997; Weiss *et al.*, 2005), flux and divergence (Nave, 1999), oscillation mode and exposure per frame, detector response and data-collection temperature (Haas & Rossmann, 1970; Young *et al.*, 1990; Young & Dewan, 1993; Hanson *et al.*, 1999, 2002; Weik *et al.*, 2001; Teng & Moffat, 2002). It also depends upon parameters of the crystal itself, including the crystal size and shape (Hedman *et al.*, 1985; Nave & Hill, 2005), the unit-cell size and symmetry, the number of molecules per asymmetric unit, the initial crystal order (mosaicity and resolution), the concentrations of solvent, salts, cryoprotective agents and heavy atoms, the X-ray absorption coefficients of the constituent atoms (for an example, see Murray *et al.*, 2004) and the chemical affinities between the constituent molecules and various radiolytic products. The amount of radiation damage that researchers report also depends upon how radiation damage is defined and measured.

Radiation damage at cryogenic temperatures mainly arises from 'primary' damage processes (Nave, 1995; Teng & Moffat, 2000; Sliz *et al.*, 2003), in which inelastic interaction of an X-ray photon with an electron in the crystal *via* the photo-

Table 1
Mass-energy absorption coefficients for lysosyme crystals as a function of iodide and chloride-ion concentration within the soaking solutions and within the crystal.

The absorption coefficients are calculated from the atomic composition of the unit cell, the size of the unit cell, the solvent content and the absorption coefficients of individual atoms at energy E_γ = 8.82 keV.

Iodide concentration in soak (M)	Chloride concentration in soak (M)	No. of iodide ions per lysozyme	No. of chloride ions per lysozyme	Mass-energy absorption coefficient μ_{en}/ρ (cm^2 g^{-1})
0.0	1.0	0.0	18.8	8.3
0.125	0.875	2.9	14.3	11.4
0.25	0.75	5.0	14.5	13.4
0.5	0.5	8.2	7.0	16.6
0.75	0.25	11.1	4.1	19.5
1.0	0.0	15.2	0.9	23.4

electric effect and (much more rarely) *via* Compton scattering results in energy deposition and bond breaking. 'Secondary' damage processes, which involve thermal diffusion and subsequent reaction of atomic and molecular radicals, are expected to be largely frozen out (Nave, 1995; Teng & Moffat, 2000; Sliz *et al.*, 2003). Previous studies have explored how radiation damage depends on the dose (energy absorbed per unit mass, proportional to the number of absorbed photons per unit mass) and dose rate (Blake & Phillips, 1962; Gonzalez & Nave, 1994; Teng & Moffat, 2000, 2002; Sliz *et al.*, 2003; Murray *et al.*, 2004). Damage is proportional to the dose at low to modest. In the absence of appreciable heating, it shows no significant dose-rate dependence over the range of fluxes available at third-generation synchrotron sources. Examination of electron-density maps has revealed preferential damage at particular sites within the protein (Weik *et al.*, 2000; Ravelli & McSweeney, 2000; Burmeister, 2000; Leiros *et al.*, 2001; Schiltz *et al.*, 2004), consistent with studies on proteins in solution (Dertinger & Jung, 1970; Box, 1972; Houee-Levin & Sicard-Roselli, 2001) and in the solid state (Baumeister *et al.*, 1976; Garrison, 1987).

Here, we examine how radiation damage at cryogenic temperatures depends upon the crystal constituents and structure, paying particular attention to the experimental details needed for the most reliably quantitative results. We examine iodide as a heavy atom not only because it has a large absorption coefficient, but also because a number of novel protein structures have recently been solved using solvent halide ions for phasing (Boggon & Shapiro, 2000; Dauter & Dauter, 2001; Evans & Bricogne, 2003). Lysozyme crystals with varying heavy-atom concentrations are irradiated and damage is determined as a function of incident photon count, total atomic absorption cross-section and total dose. These results are compared with those for crystals of catalase, thaumatin and apoferritin, which have a large range of solvent contents and molecular sizes. Our results suggest that at cryogenic temperatures the X-ray radiation-sensitivity of protein crystals, when properly defined, may be roughly independent of the crystal composition at fluxes that do not produce appreciable crystal heating.

2. Methods

2.1. Lysozyme crystal growth and halide-ion soaks

Sodium chloride, sodium iodide, cadmium sulfate, ammonium sulfate, sodium citrate dihydrate, potassium sodium tartrate tetrahydrate, glycerol (all ACS quality or better), hen egg-white lysozyme (3× recrystallized, 14.4 kDa), catalase (bovine liver, 230 kDa), thaumatin (22 kDa) and apoferritin (equine spleen, 476 kDa) were purchased from Sigma–Aldrich (St Louis, MO, USA) and used as received. Tetragonal lysozyme crystals were grown in Linbro plates by hanging-drop vapor diffusion over wells containing 1 M sodium chloride solution. For consistent final salt concentrations in the drops, plates were equilibrated for at least 4 d (equilibration time curve measured but not shown), until the drop and well concentrations matched (Diller & Hol, 1999). The crystals selected for these experiments were 400 µm in size, as assessed by their fit into the aperture of a 400 µm MicroMount (Mitegen, Ithaca, NY, USA) and had regular shapes.

The heavy-atom concentrations within these crystals were varied by exchanging chloride for iodide. Crystals were soaked in 1 M aqueous mixtures of sodium iodide and sodium chloride, with concentrations of 0.125 M iodide (I^-) and 0.875 M chloride (Cl^-), 0.25 M I^- and 0.75 M Cl^-, 0.5 M I^- and 0.5 M Cl^-, 0.75 M I^- and 0.25 M Cl^-. Each solution also contained 20 mg ml^{-1} lysozyme and 20%(w/v) glycerol as a cryoprotectant. To prevent osmotic shock, crystals to be soaked in high iodide concentrations were serially soaked in solutions of increasing concentration as listed above, remaining in each intermediate solution for roughly 5 min. To ensure consistent heavy-atom concentrations, the final soaking drop had an initial volume of exactly 60 µl and the final soak lasted 6.0 min.

2.2. Halide-ion concentration determination

To determine the number of iodide and chloride ions per lysozyme molecule taken up by each crystal, the crystal was dissolved in 1 ml water. The resulting solution was analyzed by inductively coupled plasma atomic emission spectrometry (ICP–AES; IRIS Advantage, Thermo Electron, Waltham, MA, USA) to measure the iodide concentration, by ion chromatography (IC; Dionex 500, Sunnyvale, CA, USA) to measure the chloride concentration and by UV–Vis spectrophotometry (Spectronic Genesys 5, Thermo Electron, Waltham, MA, SUA) to measure the lysozyme concentration. The results of these measurements are given in Table 1. At a 1 M ion concentration, the ratio of ions to lysozyme molecules in the soak solution is 720. From Table 1, the ratio in the crystal is smaller by a factor of 47 and 38 for iodide and chloride ions, respectively.

2.3. Solvent-atom concentration determination

To determine the solvent-atom concentration of the unit cell (see Table 2), we followed the method of Matthews (1968). Using the accepted mean protein density of $\sim$1.4 g cm^{-3} (Squire & Himmel, 1979; Quillin & Matthews, 2000), the

Table 2
Coefficients of sensitivity, $s_{AD} = (\Delta\langle u^2\rangle/\Delta D) = (\Delta B_{rel}/8\pi^2\Delta D)$, for various proteins as determined from dose curves.

Protein	Lysozyme	Catalase	Thaumatin	Apoferritin
PDB code†	1lz8	8cat	1ly0	1ier
Space group	$P4_32_12$	$P3_221$	$P4_12_12$	$F432$
MW (kDa)	14.4	230	22.2	476
Solvent content‡ (%)	39	53	56	61
Photon energy (keV)	8.82	10.0	9.26	9.66
Mass-energy absorption coefficient μ_{en}/ρ ($cm^2\ g^{-1}$)	8.3	4.3	6.0	7.0
Coefficient of sensitivity s_{AD} ($Å^2\ MGy^{-1}$)	0.012	0.012	0.018	0.017

† The unit-cell parameters and symmetry of our crystals were identical to these depositions. ‡ Calculated following the formalism of Matthews (1968).

volume occupied by solvent was determined by subtracting the protein volume from the total unit-cell volume. The number of solvent atoms per unit cell was then calculated by assuming a solvent density within the solvent-occupied volume equal to that of the final soak solution (ranging from $\sim$1.04 g cm^{-3} for a 1 *M* aqueous solution of sodium chloride to $\sim$1.11 g cm^{-3} for 1 *M* sodium iodide). The total crystal density calculated in this way compares well with the measured values of Leung *et al.* (1999).

2.4. Calculation of X-ray absorption coefficients

The X-ray absorption coefficient of each crystal (Table 2) was then calculated from the composition of the unit cell and the published absorption coefficients of each atomic constituent (Hubbell & Seltzer, 2004). The total absorption coefficient was not sensitive to the exact values of the assumed protein and light-atom solvent densities, but depended strongly upon the halogen-atom densities.

2.5. Growth and absorption coefficients for other proteins

Hexagonal catalase, tetragonal thaumatin and cubic apoferritin crystals were grown by hanging-drop vapor diffusion using 30%(*w*/*v*) sodium citrate, 1 *M* sodium potassium tartrate, and 1%(*w*/*v*) cadmium sulfate and 0.6 *M* ammonium sulfate as precipitants, respectively (McPherson, 1999). The solvent volume within the unit cell, the salt ion concentrations and the absorption coefficients were calculated as described above. The resulting absorption coefficients are given in Table 2.

2.6. X-ray beamline characteristics

X-ray diffraction data were collected using bending-magnet station F3 at the Cornell High-Energy Synchrotron Source (CHESS). Crystals were flash-cooled in liquid nitrogen and measured in a $T = 100$ K nitrogen-gas stream (Cryostream 700, Oxford Cryosystems, Devens, MA, USA). To increase the photon flux, multilayer (ML) optics (supplied by the Optics Group at the Advanced Photon Source, Argonne National Laboratory) were installed in a double-bounce geometry. Each ML consisted of 100 bilayers of tungsten and carbon with a *d*-spacing of 27 Å. The energy band-pass of the ML, measured by scanning a silicon crystal, was about 2.2% at 10 keV. The resulting flux at the crystal was 10^{12} photons $s^{-1}\ mm^{-2}$ through a collimator of $d = 300$ µm, roughly 10^3 larger than would be provided using a Si monochromator. This is somewhat smaller than that of the highest flux stations used in previous radiation-damage studies, but there is no evidence for (or physical reason to expect) a dose-rate dependence to radiation damage, at least at fluxes of up to 10^{15} photons $s^{-1}\ mm^{-2}$ that do not cause appreciable crystal heating (Sliz *et al.*, 2003). We used an X-ray energy of 8.82 keV, far from the absorption edges in our crystals. Crystals were mounted in MicroMounts (originally developed in our group; Thorne *et al.*, 2003) and diffraction data were recorded using a Quantum 4 CCD detector (ADSC, Poway, CA, USA). While the loss in energy resolution arising from the ML optics causes a minor uncertainty in determination of the unit-cell size, the diffraction pattern could be processed with *MOSFLM* (Leslie, 1992) and analyzed with the *CCP*4 crystallographic package (Collaborative Computational Project, Number 4, 1994) as described by Deacon *et al.* (1998) and Englich *et al.* (2005).

2.7. Dosing and data-collection protocol

Any variations in illuminated crystal volume during data collection introduce substantial errors in measured reflection intensities as undamaged or more weakly damaged regions of the crystal move in and out of the beam. These variations may result from crystal rotations, from beam displacements relative to the crystal or from crystal motion in the cryostream [a particular problem with CryoLoops (Hampton Research) when they are not rigidified by excess frozen liquid and with CryoLoops and LithoLoops when they are used with off-axis cryoflows]. We thus used a different data-collection method from previous radiation-damage studies to maximize the accuracy and resolution of our results.

After mounting a fresh crystal, we collected five consecutive frames, each with a 1° oscillation, rather than a full data set. The crystal was then irradiated with a much larger dose while being held stationary at $\varphi = 5°$. At the end of this 'dosing' exposure, the crystal was rotated to the original angular position ($\varphi = 0°$) and another set of five frames was collected. This procedure was iterated until the diffraction pattern visibly deteriorated ($B_{abs} \simeq 40$ $Å^2$). The duration of the dosing exposure was chosen so as to obtain at least 15 data points per dose curve. Reflection intensity statistics for each frame set were then compared with the statistics of the first set, as described in detail below.

By dosing exactly the same spot on the crystal and collecting diffraction data only within a narrow angular wedge about the dosed orientation, we ensured that the diffraction data were obtained from a uniformly damaged region. Schulze-Briese *et al.* (2005) have shown that radiation damage is limited to the exposed region of the crystal. They noted that as the crystal is rotated the center of the crystal receives a larger dose than the outer regions. Consequently, dose calculations must, in general, account for crystal rotation in

the beam. By irradiating only a narrow angular wedge, we eliminated this and other potential errors in calculating the dose. Furthermore, shifts of the beam footprint of as little as a few micrometres can cause substantial spurious trends in damage-dose curves, so we collected new data whenever beam shifts occurred. As result, we obtained excellent reproducibility and greatly reduced uncertainties from modest data sets, allowing us to reliably quantify small differences in radiation-sensitivity.

2.8. Dose calculations

The incident X-ray photon flux decayed with the beam current, with a time constant of roughly 6 h. The total number of incident photons was determined by recording the photon flux every 15 min using a calibrated ionization chamber and then integrating the resulting curve. The fraction of the incident intensity attenuated by the crystal was obtained using Beer's law,

$$\frac{I_{\rm attn}}{I_0} = 1 - \exp[-(\mu/\rho)x] \simeq (\mu/\rho)x,$$

where $x = \rho t$ is the mass thickness of the crystal, t is the crystal thickness, ρ is the mass density and (μ/ρ) is the mass attenuation coefficient (see, for example, Blundell & Johnson, 1976).

The attenuated intensity decreases approximately linearly with thickness provided that $t < 1/\mu$. For a typical protein crystal, $(\mu/\rho) \simeq 10\ {\rm cm^2\ g^{-1}}$ and $\rho \simeq 1.3\ {\rm g\ cm^{-3}}$, so $1/\mu \simeq 700\ \mu{\rm m}$, larger than the 400 µm size of our crystals. Attenuation occurs owing to both photon absorption and coherent scattering (diffraction), but only the former is relevant in calculating the dose. To obtain the absorbed intensity, we replace (μ/ρ) with the mass-energy absorption coefficient $(\mu_{\rm en}/\rho)$. This is calculated by summing over the coefficients $(\mu_{\rm en}/\rho)_i$ of each atom within the unit cell,

$$\mu_{\rm en}/\rho = \sum_i w_i(\mu_{\rm en}/\rho)_i,$$

where w_i is the fraction by weight of the ith atomic constituent, determined as described in §2.4. The dose (absorbed energy per mass) deposited in the crystal is then

$$D = \frac{N_\gamma(I_{\rm abs}/I_0)E_\gamma}{\rho V_{\rm footprint}} \simeq \frac{N_\gamma(\mu_{\rm en}/\rho)E_\gamma}{A},$$

where N_γ is the total number of photons of energy E_γ falling on the crystal within a footprint of area A on its face.

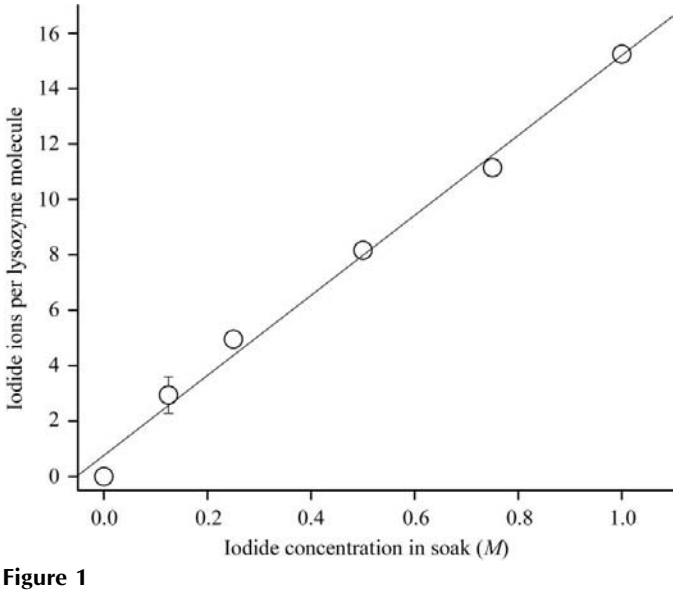

Figure 1
Number of iodide ions per molecule of lysozyme in the crystal determined by ICP–AES and UV–Vis measurements as a function of iodide concentration in the soak solution. A representative error bar is shown.

2.9. Metric of radiation-sensitivity

Metrics for radiation-sensitivity used in previous radiation-damage studies include diffraction resolution, mosaicity, unit-cell size, integrated reflection intensities and Wilson B factors. Since we wanted to compare successive measurements of the same set of reflections with our first reference set, we chose relative isotropic B factors as our metric.

Reflections after dosing were scaled relative to reflections from the fresh crystal by a modification of the method of Fox & Holmes (1966), using *SCALEIT* (Howell & Smith, 1992) from the *CCP*4 program suite (Collaborative Computational Project, Number 4, 1994). The scales are determined from a least-squares fit that minimizes the quantity

$$\sum_h \sum_s \frac{1}{\sigma_{hs}^2}(F_{hs}^2 - G_s F_h^2)^2$$

with $G_1 = 1$ and $G_2 = K_{\rm rel}^{-1}\exp(2B_{\rm rel}\sin^2\theta/\lambda^2)$, where h runs over all reflections in the set s [and $s = 1$ denotes the reference (undosed) set of reflections and $s = 2$ a dosed group], σ_{hs} is the standard deviation of reflection h in set s, F_{hs}^2 is the intensity of reflection h in set s,

$$F_h^2 = \left(\sum_m \frac{G_m}{\sigma_{hm}^2}F_{hm}^2\right) \Big/ \left(\sum_m \frac{G_m^2}{\sigma_{hm}^2}\right)$$

is the weighted mean of the reference and scaled F^2 with m denoting the reference and dosed sets, $K_{\rm rel}$ and $B_{\rm rel}$ are the scale and the relative B factor of a dosed set (for the first set $K_{\rm rel} = 1$ and $B_{\rm rel} = 0$ by definition) and θ and λ are the scattering angle and wavelength, respectively.

There are two main advantages to using relative instead of absolute B factors as metrics of radiation damage. Firstly, because we only collect data in a 5° wedge to minimize errors from non-uniform damage, there may not be enough reflections to give the intensity statistics needed to reliably determine the absolute B factors from a Wilson plot. Secondly, we want to determine B factors for crystals after they cease to diffract beyond the useful resolution limit needed for Wilson statistics (<∼3 Å). This is possible with relative B factors, since reflections are compared using *SCALEIT* with the identical reflections in subsequent sets. Plots of relative B factors *versus* dose are in fact considerably smoother than those of absolute B factors (data not shown).

The relative B factor determined by the above scaling procedure is related to the absolute isotropic B factor that can be obtained from a Wilson plot, *i.e.* from a fit to $\langle I(h)\rangle_\theta = K_{\rm abs}|F(h)|^2\exp(-2B_{\rm abs}\sin^2\theta/\lambda^2)$ by $B^i_{\rm rel} = B^i_{\rm abs} - B^{\rm ref}_{\rm abs}$, where $B^i_{\rm rel}$ is the relative B factor of the set of reflections acquired after the ith dose and $B^i_{\rm abs}$ and $B^{\rm ref}_{\rm abs}$ are the absolute B factors of the ith and the reference (undosed) set, respectively.

The Debye–Waller equation interprets the absolute B factor as a 'temperature' factor proportional to the mean-square atomic displacements, $\langle u^2\rangle = B_{\rm abs}/8\pi^2$. Although we do not measure the absolute B factors (because the assumptions in Wilson statistics do not hold for low-resolution reflections), we obtain relative B factors with good reproducibility even when crystals are barely diffracting. We interpret these relative B factors as proportional to the change in the mean-squared atomic displacements, $\Delta\langle u^2\rangle = (\Delta B_{rel})/8\pi^2$.

3. Results

Mass-energy absorption coefficients of lysozyme crystals were varied by soaking crystals in solutions containing sodium iodide. The iodide ions diffuse into 400 µm crystals within a minute of soaking (Dauter *et al.*, 2000; Dauter & Dauter, 2001). Fig. 1 shows combined ICP and UV–Vis spectrophotometry data for the number of ions per lysozyme molecule taken up by the crystal. This number varies linearly with the iodide-ion concentration in the soaking solution. At an energy of 8.82 keV, the mass-energy absorption coefficient of iodine of 215 cm^2 g^{-1} is roughly 30 times larger than that of oxygen and 70 times larger than that of carbon. At the measured concentrations within the crystal, it dominates the total mass-energy absorption coefficient. Table 1 gives the calculated total mass-energy absorption coefficients for crystals soaked in solutions with iodide concentration of up to 1 M (obtained by adding contributions from lysozyme, solvent, salt ions and cryoprotectant). These coefficients vary from 8.31 cm^2 g^{-1} (no iodide) to 23.4 cm^2 g^{-1} (1 M iodide soak).

Typical diffraction spots acquired from a lysozyme crystal using ML optics (not shown) were radially streaked because of the convolution of wavelength spread, beam divergence and crystal mosaicity. However, the spots are well separated and could be processed using *MOSFLM* (with a large fixed integration box) and the *CCP*4 program suite as described by Deacon *et al.* (1998) and in §2.6. Although the unit-cell parameters and symmetry could be identified unambiguously, uncertainties introduced by the ML prevented accurate measurements of unit-cell expansion and mosaic broadening caused by radiation damage.

Fig. 2 shows the change in relative B factor *versus* the number of photons per square millimetre incident upon the crystal (*i.e. versus* the photon fluence or time-integrated flux)

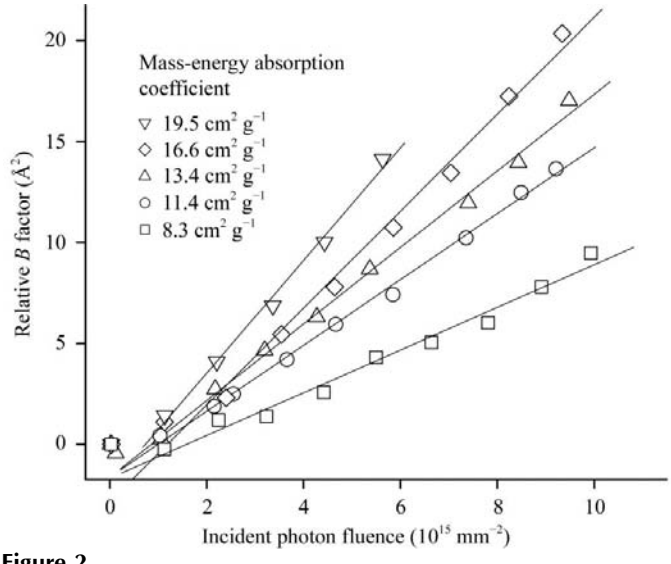

Figure 2
Relative B factor *versus* incident fluence (photons mm^{-2}) at E = 8.8 keV for lysozyme crystals that have been soaked in varying concentrations of sodium iodide. Radiation damage per incident photon is greater for crystals containing larger iodide concentrations.

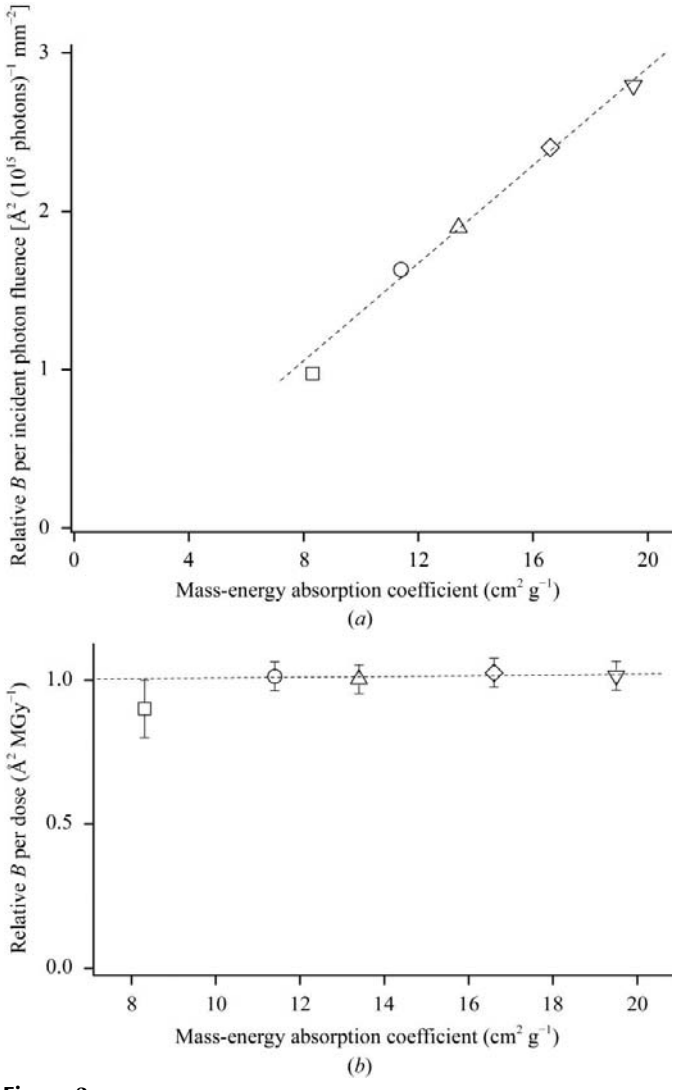

Figure 3
Change in relative B factor (*a*) per incident photon fluence and (*b*) per dose at E = 8.8 keV *versus* mass-energy absorption coefficient for lysozyme crystals soaked in solutions with iodide concentrations of 0 M (squares), 0.125 M (circles), 0.25 M (triangles), 0.5 M (diamonds) and 0.75 M (inverted triangles).

for lysozyme crystals having five different I^- concentrations and thus different mass-energy absorption coefficients. The data are linear, consistent with previous results for lysozyme that used other damage metrics (Teng & Moffat, 2000, 2002). The scatter in the data is very small despite the relatively small data sets analyzed, indicating the utility of our data-collection protocol and damage metric.

Fig. 3(*a*) shows the change in relative *B* factors per 10^{15} photons mm^{-2}, obtained from the slopes of the linear fits in Fig. 2, *versus* the crystal's mass-energy absorption coefficient. Damage per impinging photon depends linearly on the absorption coefficient. Fig. 3(*b*) shows that the change in relative *B* factors per dose (*i.e.* per absorbed photon) is independent of absorption coefficient. In other words, an equal amount of energy delivered per mass of crystal causes the same amount of damage, regardless of the crystal composition. Each crystal's diffraction degraded to $B_{\rm abs} > 40$ Å^2 after absorbing a dose of about 20 MGy, consistent with Henderson's estimate (Henderson, 1990) and the early experiments of Blake and Phillips (1962).

Using our finding that the relative *B* factors increase linearly with absorbed dose, we define a 'coefficient of sensitivity to absorbed dose' as $s_{\rm AD} = (\Delta B_{\rm rel}/\Delta D 8\pi^2)$. This coefficient relates the increase in mean-squared atomic displacements (as defined in §2.9) to the dose ΔD, $\Delta\langle u^2\rangle = s_{\rm AD}\Delta D$. Table 2 gives $s_{\rm AD}$ for crystals of lysozyme of varying absorption coefficients. $s_{\rm AD} \simeq 0.012$ Å^2 MGy^{-1}, regardless of iodine concentration.

Similar measurements have been performed on native (*i.e.* unsoaked) crystals of catalase, thaumatin and apoferritin. These crystals span a range of molecular weights (230, 22 and 476 kDa compared with 14 kDa for lysozyme) and solvent contents (53, 56 and 61% compared with 39% for tetragonal lysozyme). Fig. 4 shows their response curves (change in relative *B* factor *versus* dose), which are also linear, and Table 2 gives their coefficients of sensitivity. For catalase, a protein that has been reported as being particularly radiation-sensitive (McPherson & Rich, 1973), the coefficient is the same as for lysozyme, while thaumatin and apoferritin have somewhat larger coefficients. These very limited results suggest that most protein crystals (perhaps excluding those with the highest solvent contents, where solvent and small-molecule solutes dominate the total absorption cross-section) may show similar radiation damage per unit dose at cryogenic temperatures, consistent with findings in cryoelectron diffraction (Henderson, 1990). Variations in radiation-sensitivity per coherently scattered photon are primarily a consequence of variations in absorption cross-section and not of details of sequence, structure and packing beyond their effect on absorption cross-section.

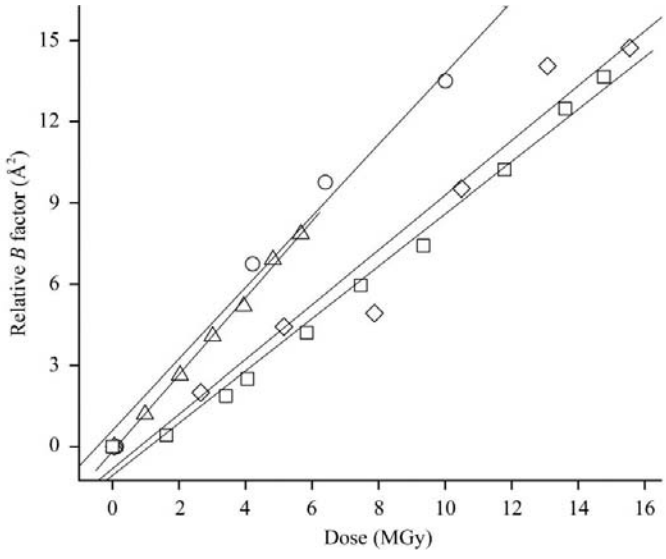

Figure 4
Change in relative *B* factor *versus* dose at energies listed in Table 2 for crystals of lysozyme (squares), catalase (diamonds), thaumatin (triangles) and apoferritin (circles).

4. Discussion

4.1. Quantifying radiation damage

Accurately quantifying radiation damage is essential to understanding the mechanisms by which it occurs and to evaluating possible approaches to reducing its effects. This is especially true at cryogenic temperatures ($T \leq 140$ K). The preponderance of evidence to date, from both protein crystallography and cryoelectron microscopy, suggests that at cryogenic temperatures protein-to-protein variability in sensitivity per unit dose is small. Apparently inconsistent results for the effects of data-collection temperature below $T = 140$ K (Hanson *et al.*, 1999, 2002; Teng & Moffat, 2002) and of radical scavengers (Murray & Garman, 2002; Kmetko & Thorne, 2006) indicate that the effects of temperature and scavengers must also be small. On the other hand, commonly used metrics of radiation damage such as diffraction resolution, *B* factors and unit-cell size are the result of fitting procedures that are sensitive to many factors beyond the actual order of the crystal and whose details are generally obscure to those of us who use standard analysis packages. For example, some studies have found a simple correlation between unit-cell volume and dose (Burmeister, 2000; Teng & Moffat, 2000; Ravelli *et al.*, 2002), whereas another found large crystal-to-crystal variations for the same protein (Murray & Garman, 2002). We suspect this is a consequence of differences in data-collection and analysis protocols rather than of the actual behavior of the crystals.

For all the data sets collected in the present study, using different heavy-ion concentrations and different proteins, the relative *B* factor shows a simple linear dependence on dose. The curves show little scatter, even though the number of reflections collected and analyzed is much smaller than in previous studies. The relative *B* factor has the additional merit of a straightforward connection to the measured reflection intensities. This suggests that our metric of relative isotropic *B* factor combined with our data-collection protocol, which guarantees uniform dosing of the irradiated volume and data collection from that same volume, can yield the reproducibility and resolution needed for systematic radiation-damage studies at cryogenic temperatures.

4.2. Effects of salts

In some cases, factors of two in radiation-sensitivity can be crucial in collecting a complete data set from a single crystal. Our results indicate that sensitivity increases of this magnitude may be produced by commonly used salts that have large atomic number constituents (*e.g.* S, Cl, K, Ca, I), especially in high solvent-content crystals. As previously suggested (Murray *et al.*, 2004) and as is well known from experience with heavy-atom derivatives, damage may be reduced by growing crystals using salts with lower atomic number constituents or by removing offending atoms by soaking after growth and prior to data collection.

4.3. Local *versus* average damage

In addition to average effects on structure measured by, for example, absolute or relative B factors, recent experiments (Weik *et al.*, 2000; Ravelli & McSweeney, 2000; Burmeister, 2000; Leiros *et al.*, 2001; Schiltz *et al.*, 2004) have shown that X-ray absorption produces site-specific damage such as broken disulfide bonds. The kinds of damage seen and the residues affected are consistent with previous studies of radiation damage in solution and in dry proteins (Dertinger & Jung, 1970; Box, 1972; Houee-Levin & Sicard-Roselli, 2001), which have identified 'magnets' (generally weak bonds) to which the products of X-ray absorption are drawn. Although this site-specific damage has consequences for interpreting X-ray structures, there are important caveats. The appearance at low doses of damage to these sites may also be a consequence of their location in well constrained and well ordered parts of the protein. For a broken bond to become visible in the electron-density map, it must be reproducibly broken in a substantial fraction of unit cells and the broken pieces must adopt a similar conformation. Less constrained and less-well ordered regions may adopt a broader range of conformations before and/or after damage and so their damage may remain invisible, except in global measures such as the B factor or unit-cell volume, until they are damaged in a much larger fraction of unit cells.

4.4. Primary *versus* secondary damage

The present results show a simple scaling of damage with absorption cross-section in iodine-containing lysozyme crystals and a relatively small (less than factor-of-two) variation in radiation-sensitivity per unit dose for four proteins. The model proteins studied span a range of molecular weights and solvent contents and those with the highest solvent contents (thaumatin and apoferritin) contain a significant fraction of bulk-like solvent. This suggests that damage *versus* dose at $T = 100$ K is largely independent (*i.e.* to within a factor of two) of the structural details of the protein and how it is packed within the unit cell, which is consistent with experience in cryoelectron diffraction on proteins (Henderson, 1990) and with the few published X-ray diffraction experiments where damage at well defined doses (as opposed to, for example, exposure times or incident photon fluences) has been reported (Blake & Phillips, 1962; Helliwell, 1988; Burmeister, 2000; Teng & Moffat, 2000; Ravelli & McSweeney, 2000; Leiros *et al.*, 2001, 2006; Owen *et al.*, 2006).

This conclusion suggests that degradation of diffraction at $T = 100$ K and at doses well below those at which diffraction disappears arises almost entirely from primary radiation-damage processes, *i.e.* to processes that do not involve the thermal diffusion of atomic and molecular radicals and the larger scale conformational and lattice changes they can produce. Secondary damage processes, which are responsible for the enormous increase in radiation-sensitivity on warming from below the glass transition of water at $T \simeq 150$ K to room temperature, have an effect at $T = 100$ K (constrained by our estimated factor of two uncertainty in protein-to-protein variability) that is at most comparable in magnitude to primary processes and is likely to be much smaller. An even stronger constraint on the importance of secondary damage processes can be provided by data collection at lower temperatures. X-ray diffraction measurements at $T = 16$ K (Hanson *et al.*, 1999, 2002) and at $T = 40$ K (Teng & Moffat, 2002) showed small (less than a factor of two) reductions in damage rates relative to $T = 100$ K. XANES measurements on a metalloprotein showed reductions in damage to the metal site of roughly a factor of two on cooling from $T = 100$ K to $T = 10$ K (Yano *et al.*, 2005). Results of other studies at lower temperatures have been inconclusive (Garman & Owen, 2006). In any case, it is not obvious how the effect of diffusive/thermally activated processes could change so little on reduction of absolute temperature by a factor of 2.5 to 10. It also seems obvious that primary damage should show some small temperature dependence (for example, through parameters that depend on mean interatomic distances) on cooling below $T = 100$ K.

X-ray energy is absorbed by the photoelectric effect and to a lesser extent Compton scattering by atoms within the crystal, leading to ejection of highly energetic electrons. Energy-transfer processes involving these electrons eventually produce several hundred radicals per absorbed X-ray photon in $<<10^{-6}$ s in a volume of dimension $\sim$30 Å (von Sonntag, 1987; Draganic & Draganic, 1971). The most important of these radicals include solvated electrons, hydroxyl radicals, hydroperoxyl radicals, oxygen radicals and hydrogen radicals produced by radiolysis of water and hydrogen radicals from the macromolecule itself (Draganic & Draganic, 1971; Bensasson *et al.*, 1993). Because the solvent is frozen at cryogenic temperatures, diffusion and subsequent reaction of atomic and molecular free radicals is all but eliminated. The rigid solvent network also prevents changes in secondary and higher level structure owing to local damage as well as displacements and rotations of the molecule as a whole that could otherwise produce much larger degradation of diffraction than local damage. Based on this discussion, there is little reason to expect substantial (*e.g.* order-of-magnitude) protein-to-protein variations in radiation damage per absorbed photon at cryogenic temperatures. The same dose should produce roughly the same amount of local damage. Because of the rigid solvent network, differences in conformational flex-

ibility, solvent content and crystal packing should be largely irrelevant.

How then can we account for the common belief that some proteins are much more easily damaged by X-rays than others at $T = 100$ K? What is typically noted is how many frames can be acquired with good intensity statistics before diffraction fades (Glaeser *et al.*, 2000). Actual photon fluences (time-integrated incident fluxes) at which damage becomes significant have rarely been measured and doses have been estimated only in the handful of studies cited earlier, which show consistent damage rates. Actual doses (energy absorbed per unit mass) depend upon the fluence, the protein's composition (usually known), the ion types within the crystal (sometimes known), the ion concentrations within the crystal (usually unknown, because they are very different from those in the mother liquor or soak solution and because not all ions are sufficiently ordered to appear in electron-density maps) and the proximity of the X-ray energy to absorption edges of the crystal's constituent atoms. There are ample uncertainties to account for the perceived behavior.

Crystals with large unit cells must scatter (and absorb) many more photons per unit mass to achieve the same reciprocal-space peak intensities. For fixed crystal quality, the dose received in acquiring a data set with given intensity statistics scales with cell volume (Glaeser *et al.*, 2000; Blundell & Johnson, 1976) (if diffuse background from solvent and gas in the X-ray beam path can be ignored; both are cell-volume independent and so cause I/σ at a fixed resolution to drop as cell size grows). Consequently, damage incurred per frame should scale roughly with cell volume. Similarly, damage incurred per frame scales inversely with crystal volume. Proteins whose crystals are small or whose cell volumes are large may thus seem more radiation-sensitive. The rate of damage with dose in initially well ordered crystals increases rapidly once diffraction (and thus order) has degraded beyond a certain point (Blake & Phillips, 1962). Consequently, in crystals with poor initial order, the less rigid constraints and additional 'elbow-room' provided by, for example, molecule-to-molecule conformation and orientation variations and by gaps between mosaic grains may allow damage to occur more rapidly.

Even more important may be the much higher ion concentrations expected within some disordered crystals. Experiments on tetragonal lysozyme crystals (Vekilov *et al.*, 1996), including our own unpublished work, show that small (<50 µm) crystals can have 4–10 times the salt-ion concentrations of large crystals. These excess concentrations are correlated with heterogeneous nucleation that leads to protein impurity-rich cores with high defect densities (Vekilov *et al.*, 1996; Caylor *et al.*, 1999). As the crystal grows larger, impurity concentrations drop, the average quality improves and ion concentrations asymptote to bulk values. Even for a relatively benign (*i.e.* small absorption cross-section) salt such as NaCl, such impurity-induced ion-concentration enhancements could easily double the total absorption cross-section of a crystal. In the presence of this impurity and salt 'coring', small crystals of a given protein will tend to have larger mass-energy absorption coefficients and suffer more damage for fixed incident fluence than large ones.

4.5. Site-specific damage

Site-specific damage to proteins evident in electron-density maps has been interpreted as evidence of the importance of secondary damage processes. For example, it has been suggested that if primary damage dominates, then site-specific damage should be greatest at sites with the largest atomic absorption cross-section, which is contrary to observation (Garman & Owen, 2006). However, the hundreds of electrons produced by the initial photoelectric absorption event are dispersed far from the absorbing atom and thus can cause damage at distances that are large compared with the typical size of preferentially damaged regions. More important, transfer of these excited electrons along the protein backbone to 'magnet' sites where they preferentially break bonds requires only the energy imparted by the initial absorption event. ESR studies have shown this to occur at high rates at liquid-helium temperatures (Jones *et al.*, 1987; Symons, 1995, 1997). Although 'secondary damage' is somewhat ill-defined, a pragmatic definition based on its conventional use in the broader radiation-damage community is damage caused by processes involving thermal diffusion of atoms and larger radical species, *i.e.* involving thermal mass (and not just electronic) transport. While hydroxyl radicals may be somewhat thermally mobile at $T = 77$ K, their mobility is likely to be too small to account for the observed site-specific damage. Motion of excited electrons by athermal processes (*e.g.* tunneling) and by thermal hopping is likely to dominate in producing 'remote' damage at these temperatures. This conjecture and the relative importance of athermal and thermal electron transport can be tested by comparing site-specific damage in X-ray structures determined at, for example, $T = 100$ K and $T = 4$ K as a function of total dose.

5. Conclusion

We have defined a data-collection protocol and a coefficient of sensitivity to absorbed dose that provide a robust and reliable measure of damage. This coefficient is constant to within a factor of two for proteins with substantially different molecular weights and solvent contents, supporting the notion that all protein crystals may be comparably radiation-sensitive at temperatures used in cryocrystallography. Our methods should prove particularly useful for fast accurate screening of protein crystal radiation-sensitivities.

Finally, since submission of our manuscript Owen *et al.* (2006) have reported similar radiation damage per absorbed dose for apoferritin and holoferritin.

The authors would like to thank Dr Renuka Rao of Cornell Nutrient Analysis Laboratory for assisting with the ICP and IC measurements, Dr Qun Shen and Dr Andrew Stewart of CHESS for helping at the F3 station and Drs Marian Szebenyi and Ulrich Englich of MacCHESS for helpful discussion. This

work was funded by the National Institutes of Health (R01 GM65981). CHESS and MacCHESS are respectively supported by the National Science Foundation (DMR 97-13424) and by the NIH through its National Center for Research Resources (RR-01646).

References

Arndt, U. W. (1984). *J. Appl. Cryst.* **17**, 118–119.

Baumeister, W., Hahn, M. & Seredynski, J. (1976). *Ultramicroscopy*, **1**, 377–382.

Bensasson, R. V., Land, E. J. & Truscott, T. G. (1993). *Excited States and Free Radicals in Biology and Medicine: Contributions from Flash Photolysis and Pulse Radiolysis.* Oxford University Press.

Blake, C. C. F. & Phillips, D. C. (1962). *Biological Effects of Ionizing Radiation at the Molecular Level*, pp. 183–192. Vienna: International Atomic Energy Agency.

Blundell, T. L. & Johnson, L. N. (1976). *Protein Crystallography*. New York: Academic Press.

Boggon, T. J. & Shapiro, L. (2000). *Structure*, **8**, R143–R149.

Box, H. C. (1972). *Annu. Rev. Nucl. Part. Sci.* **22**, 355–382.

Burmeister, W. P. (2000). *Acta Cryst.* D**56**, 328–341.

Caylor, C. L., Dobrianov, I., Lemay, S. G., Kimmer, C., Kriminski, S., Finkelstein, K. D., Zipfel, W., Webb, W. W., Thomas, B. R., Chernov, A. A. & Thorne, R. E. (1999). *Proteins*, **36**, 270–281.

Collaborative Computational Project, Number 4 (1994). *Acta Cryst.* D**50**, 760–763.

Dauter, Z. & Dauter, M. (2001). *Structure*, **9**, R21–R26.

Dauter, Z., Dauter, M. & Rajashankar, K. (2000). *Acta Cryst.* D**56**, 232–237.

Deacon, A. M., Appleby, T., Bilderback, D. H., Ealick, S. E., Fontes, E. & Thiel, D. J. (1998). *J. Synchrotron Rad.* **5**, 494–496.

Dertinger, H. & Jung, H. (1970). *Molecular Radiation Biology*. New York: Springer–Verlag.

Diller, D. & Hol, W. (1999). *Acta Cryst.* D**55**, 656–663.

Draganic, I. G. & Draganic, Z. D. (1971). *The Radiation Chemistry of Water.* New York: Academic Press.

Englich, U., Kazimirov, A., Shen, Q., Bilderback, D. H., Gruner, S. M. & Hao, Q. (2005). *J. Synchrotron. Rad.* **12**, 345–348.

Evans, G. & Bricogne, G. (2003). *Acta Cryst.* D**59**, 1923–1929.

Fox, G. & Holmes, K. (1966). *Acta Cryst.* **20**, 886–891.

Garman, E. & Nave, C. (2002). *J. Synchrotron Rad.* **9**, 327–328.

Garman, E. F. & Owen, R. L. (2006). *Acta Cryst.* D**62**, 32–47.

Garrison, W. M. (1987). *Chem. Rev.* **87**, 381–398.

Glaeser, R., Facciotti, M., Walian, P., Rouhani, S., Holton, J., MacDowell, A., Celestre, R., Cambie, D. & Padmore, H. (2000). *Biophys. J.* **79**, 3178–3185.

Gonzalez, A. & Nave, C. (1994). *Acta Cryst.* D**50**, 874–877.

Haas, D. J. & Rossmann, M. G. (1970). *Acta Cryst.* B**26**, 998–1004.

Hanson, B. L., Harp, J. M., Kirschbaum, K., Schall, C. A., DeWitt, K., Howard, A., Pinkerton, A. A. & Bunick, G. J. (2002). *J. Synchrotron Rad.* **9**, 375–381.

Hanson, B. L., Martin, A., Harp, J. A., Parrish, D. A., Kirschbaum, K., Bunick, C. G., Pinkerton, A. A. & Bunick, G. J. (1999). *J. Appl. Cryst.* **32**, 814–820.

Hedman, B., Hodgson, K. O., Helliwell, J. R. & Liddington, R. (1985). *Proc. Natl Acad. Sci. USA*, **82**, 7604–7607.

Helliwell, J. (1988). *J. Cryst. Growth*, **90**, 259–272.

Henderson, R. (1990). *Proc. R. Soc. Lond. B*, **241**, 6–8.

Houee-Levin, C. & Sicard-Roselli, C. (2001). *Radiation Chemistry: Present Status and Future Trends*, edited by C. D. Jonah & B. S. M. Rao, pp. 553–584. Amsterdam: Elsevier.

Howell, L. & Smith, D. (1992). *J. Appl. Cryst.* **25**, 81–86.

Hubbell, J. & Seltzer, S., (2004). *Tables of X-ray Mass Attenuation Coefficients and Mass Energy-Absorption Coefficients*, v.1.4. Gaithersburg, MD, USA: National Institute of Standards and Technology. http://physics.nist.gov/xaamdi.

Jones, G. D. D., Lea, J. S., Symons, M. C. R. & Taiwo, F. A. (1987). *Nature (London)*, **330**, 772–773.

Kmetko, J. & Thorne, R. E. (2006). In preparation.

Leiros, H.-K. S., McSweeney, S. M. & Smalås, A. O. (2001). *Acta Cryst.* D**57**, 488–497.

Leiros, H.-K. S., Timmins, J., Ravelli, R. B. G. & McSweeney, S. M. (2006). *Acta Cryst.* D**62**, 125–132.

Leslie, A. G. W. (1992). *Jnt CCP4/ESF–EAMCB Newsl. Protein Crystallogr.* **26**.

Leung, A. K., Park, M. M. & Borhani, D. W. (1999). *J. Appl. Cryst.* **32**, 1006–1009.

McPherson, A. (1999). *Crystallization of Biological Molecules.* Cold Spring Harbor, NY, USA: Cold Spring Harbor Laboratory Press.

McPherson, A. & Rich, A. (1973). *Arch. Biochem. Biophys.* **157**, 23–27.

Matthews, B. W. (1968). *J. Mol. Biol.* **33**, 491–497.

Murray, J. & Garman, E. (2002). *J. Synchrotron Rad.* **9**, 347–354.

Murray, J. W., Garman, E. F. & Ravelli, R. B. (2004). *J. Appl. Cryst.* **37**, 513–522.

Nave, C. (1995). *Radiat. Phys. Chem.* **45**, 483–490.

Nave, C. (1999). *Acta Cryst.* D**55**, 1663–1668.

Nave, C. & Garman, E. F. (2005). *J. Synchrotron Rad.* **12**, 257–260.

Nave, C. & Hill, M. A. (2005). *J. Synchrotron Rad.* **12**, 299–303.

Owen, R. L., Rudiño-Piñera, E. & Garman, E. F. (2006). *Proc. Natl Acad. Sci. USA*, **103**, 4912–4917.

Polikarpov, I., Teplyakova, A. & Oliva, G. (1997). *Acta Cryst.* D**53**, 734–737.

Quillin, M. L. & Matthews, B. W. (2000). *Acta Cryst.* D**56**, 791–794.

Ravelli, R. B. G. & McSweeney, S. M. (2000). *Structure*, **8**, 315–328.

Ravelli, R. B. G., Theveneau, P., McSweeney, S. & Caffrey, M. (2002). *J. Synchrotron Rad.* **9**, 355–360.

Schiltz, M., Dumas, P., Ennifar, E., Flensburg, C., Paciorek, W., Vonrhein, C. & Bricogne, G. (2004). *Acta Cryst.* D**60**, 1024–1031.

Schulze-Briese, C., Wagner, A., Tomizaki, T. & Oetiker, M. (2005). *J. Synchrotron Rad.* **12**, 261– 267.

Sliz, P., Harrison, S. C. & Rosenbaum, G. (2003). *Structure*, **11**, 13–19.

Sonntag, C. von (1987). *The Chemical Basis of Radiation Biology.* London: Taylor & Francis.

Squire, P. & Himmel, M. (1979). *Arch. Biochem. Biophys.* **196**, 165–177.

Symons, M. C. R. (1995). *Radiat. Phys. Chem.* **45**, 837–845.

Symons, M. C. R. (1997). *Free Radic. Biol. Med.* **22**, 1271–1276.

Teng, T.-Y. & Moffat, K. (2000). *J. Synchrotron Rad.* **7**, 313–317.

Teng, T.-Y. & Moffat, K. (2002). *J. Synchrotron Rad.* **9**, 198–201.

Thorne, R. E., Stum, Z., Kmetko, J., O'Neill, K. & Gillilan, R. (2003). *J. Appl. Cryst.* **36**, 1455–1460.

Vekilov, P. G., Monaco, L. A., Thomas, B. R., Stojanoff, V. & Rosenberger, F. (1996). *Acta Cryst.* D**52**, 785–798.

Weik, M., Ravelli, R. B., Kryger, G., McSweeney, S., Raves, M. L., Harel, M., Gros, P., Silman, I., Kroon, J. & Sussman, J. L. (2000). *Proc. Natl Acad. Sci. USA*, **97**, 623–628.

Weik, M., Ravelli, R. B., Silman, I., Sussman, J. L., Gros, P. & Kroon, J. (2001). *Protein Sci.* **10**, 1953–1961.

Weiss, M. S., Panjikar, S., Mueller-Dieckmann, C. & Tucker, P. A. (2005). *J. Synchrotron Rad.* **12**, 304–309.

Yano, J., Kern, J., Irrgang, K., Latimer, M., Bergmann, U., Glatzel, P., Pushkar, Y., Biesiadka, J., Loll, B., Sauer, K., Messinger, J., Zouni, A. & Yachandra, V. (2005). *Proc. Natl Acad. Sci. USA*, **102**, 12047–12052.

Young, A. C. & Dewan, J. C. (1993). *J. Appl. Cryst.* **26**, 309–319.

Young, A. C., Dewan, J. C., Thompson, A. W. & Nave, C. (1990). *J. Appl. Cryst.* **23**, 215–218.